SCIENTIFIC REPORTS

OPEN

Enhanced Optical Properties of ZnO and CeO$_2$-coated ZnO Nanostructures Achieved Via Spherical Nanoshells Growth On A Polystyrene Template

Asmaa Eltayeb[ID][1], Stephen Daniels[1] & Enda McGlynn[2]

In this paper, ZnO, CeO$_2$ and CeO$_2$-coated ZnO nanostructures were synthesised by simple and efficient low temperature wet chemical methods on Si (100) and quartz substrates. The ZnO films were prepared by a drop coating deposition method. This was then combined with a thin layer of the redox active material CeO$_2$ to form CeO$_2$-coated ZnO films. Spherical ZnO nanoshell structures and CeO$_2$-coated ZnO nanoshells have been prepared using polystyrene (PS) sphere monolayer templates. The structural properties and morphologies of the nanostructures were analysed by x-ray diffraction (XRD) and scanning electron microscopy (SEM). The nanostructure compositions are studied in more detail using secondary ion mass spectroscopy (SIMS). The optical properties of the nanostructures were measured using ultraviolet-visible (UV-Vis) absorption spectroscopy in order to ascertain the effects of the nanoshell structures and the whispering gallery modes associated with these structures on the optical properties of the deposits. Our data show UV and visible light absorption was very significantly enhanced due to this nanostructuring.

Enhanced broadband light absorption by nanostructuring of materials, recently described by Yao et al.[1]., is considered an important new engineering design parameter for high performance solar cells and protectors. This new method of light management uses low quality factor whispering gallery resonant modes inside spherical nanoshell structures where the geometry of the structure dramatically improves the absorption and reduces adverse directionality effects due to the substantial enhancement of the effective light path in the active material[2, 3]. Applying this important recent development in conjunction with a redox mediator and a UV absorber, such as CeO$_2$ and ZnO[4, 5], can result in enhancement in the UV light absorption and optical properties, which can in turn be used for more effective applications in a variety of technologies, especially given the relatively favourable band alignment for charge transfer, with a likely small contact potential (see Supplementary Figure I).

Materials based on CeO$_2$ are extensively used in many applications including oxygen ion conduction in solid oxide fuel cells[6], UV absorption[5, 7], two step thermochemical cycling[8] and gas sensing[9]. Apart from the well-known oxygen storage capacity of CeO$_2$ and its redox properties, CeO$_2$ is also suitable for many personal care products specifically related to its ability to block ultraviolet radiation[10–12]. Similarly, ZnO is an important and promising material with many potential applications in short-wavelength optoelectronic and other devices[13], such as transparent conductive films, surface electro-acoustic wave devices, ultraviolet emitters, cold cathode emitters etc. It has a wide and direct bandgap energy of 3.3 eV at room temperature[14] and many useful properties such as transparency in the visible range, electrochemical stability and non-toxicity[15, 16]. Therefore, combining both materials (ZnO and CeO$_2$) can result in a material with enhanced/unique UV absorption and high stability at high temperature and high material hardness[5].

[1]School of Electronic Engineering, National Centre for Plasma Science and Technology, Dublin City University, Glasnevin, Dublin 9, Ireland. [2]School of Physical Sciences, National Centre for Plasma Science and Technology, Dublin City University, Glasnevin, Dublin 9, Ireland. Correspondence and requests for materials should be addressed to A.E. (email: asmaa.eltayeb2@mail.dcu.ie)
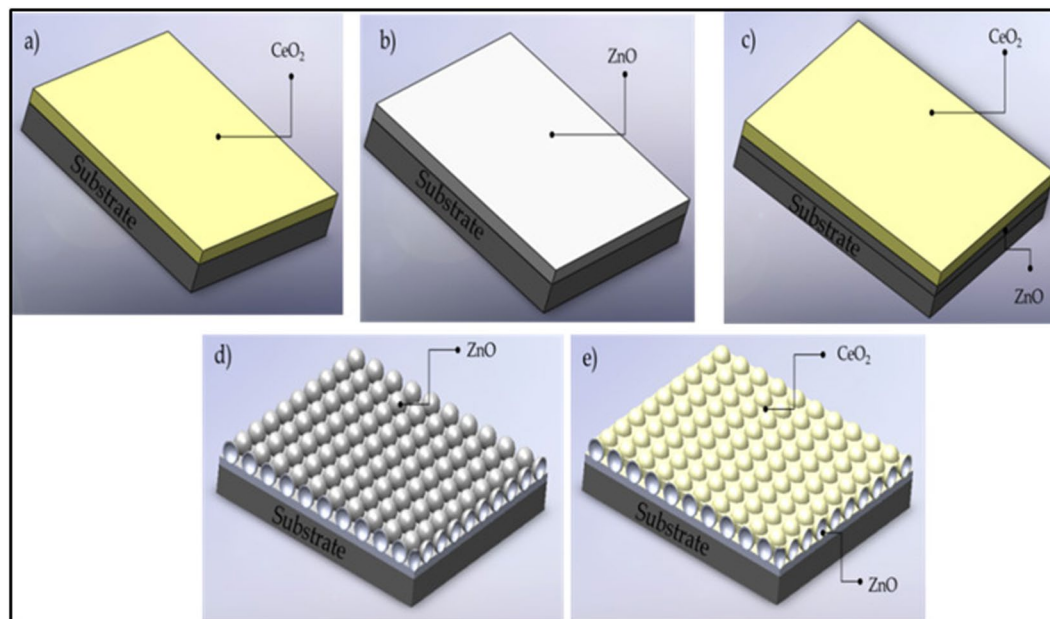
Figure 1. Morphologies used in this study: (**a**) CeO$_2$, (**b**) ZnO and (**c**) CeO$_2$-coated ZnO films, and; (**d**) ZnO and (**e**) CeO$_2$-coated ZnO spherical nanoshells. All samples were deposited on both Si (100) and quartz substrates.

ZnO nanostructures have recently attracted a great attention due to their interesting properties for photonic applications and the variety of morphological structures which can be achieved including nanorods[17], nanorings[18], nanowires[19] and nanobelts[20]. Among these various structures, hollow nanostructures are interesting structures for applications such as photocatalysis[21], solar cells[22], drug delivery[23] and much more[24–26]. Synthesising hollow ZnO nanostructures has been recently done using various templates. For example, Sun et al.[27–29] report extraordinary visible-light responses for ZnO hollow microsphere structures synthesised by their recently developed two-step self-assembly concept. These interesting studies were inspired by examples from the biological realm, including the fly compound-eye and fish-scale structures. Jiang et al. synthesised ZnO hollow spheres using ethanol droplets as soft templates while Neves et al. synthesised ZnO hollow spheres by coating polystyrene beads. Others, like Li et al.[30], Shen et al.[31] and Deng et al.[32], synthesised ZnO hollow particles using a template-free solution method, template-free evaporation method and template-free sonochemical fabrication method, respectively. Although these proposed methods are described as simple and inexpensive, the drop coating method (proposed by Byrne et al.[17, 33]) using a template of polystyrene beads, yields samples with a patterned spherical nanoshells of ZnO with improved crystallinity, purity and optical properties.

The aim of the present study is to engineer patterned spherical nanoshells of ZnO coated with a CeO$_2$ film to achieve enhanced optical properties (UV absorption) primarily for solar-thermal-related applications. The samples used in this study are shown in Fig. 1. The ZnO-CeO$_2$ nanostructures were synthesised by drop coating and pulsed DC magnetron sputtering and characterised by XRD, SEM, SIMS and UV-Vis spectroscopy. To the best of our knowledge, using drop coating of PS sphere templates to engineer patterned spherical nanoshells of ZnO has not been reported previously, and is a very simple and versatile method. Our work provides useful information on the influence of the nanoshell geometry on the absorption properties of various combinations of these two types of materials. The addition of the CeO$_2$ thin film on top of the ZnO hollow nanostructured deposit enhances the UV light absorption further and provides additional functionality such as oxygen storage capacity via changes in stoichiometry. The redox properties of these types of CeO$_2$ films grown in our group were reported in ref. 34.

Experimental

Material Synthesis. Prior to deposition, Si(100) and quartz substrates were cleaved to the desired size (2 × 2 cm) and the substrates were ultrasonically cleaned using acetone and a decontamination solution (30905 Aldrich) and then rinsed with deionised water and blown dry with a nitrogen stream. The ZnO layers used to generate ZnO films were prepared by a method initially proposed and demonstrated by Greene et al.[35, 36] and further developed by Byrne et al.[17, 33, 37]. This method involves drop coating a mixture of zinc acetate (5 mM) in anhydrous ethanol solution onto the substrate surface for a period of 20–25 seconds before being rinsed with fresh ethanol and dried with a nitrogen stream. This process was repeated approximately 60 times (1 time yields approximately a film thickness of 2 nm). The substrates were then annealed at 350 °C for 20 minutes, yielding a uniform textured nanocrystalline ZnO film with a film thickness of 120 ± 10 nm. Patterned spherical ZnO nanoshells were fabricated on a PS sphere template using the same deposition method for the ZnO films. A monolayer of the PS spheres with a diameter of ca. 600 nm (solid content of ~10 wt.%, Fisher Scientific) were generated by a self-assembly process on the surface of DI water, at room temperature, and then transferred onto bare substrates[33]. The

2

Sample Label	Sample Structure Description
C_F	CeO$_2$ Films
Z_F	ZnO Films
C_Z_F	CeO$_2$-coated ZnO Films
Z_NS	ZnO Nanoshells
C_Z_NS	CeO$_2$-coated ZnO Nanoshells

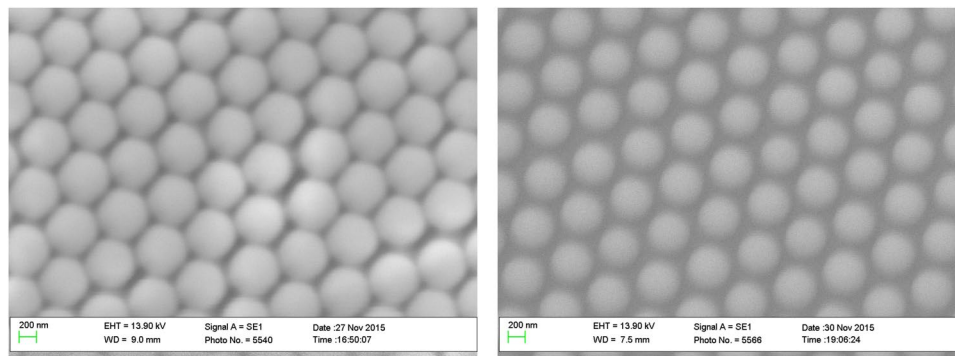**Table 1.** Associated labels for sample structures used in this study.

Figure 2. SEM images of the polystyrene sphere monolayer deposited on a Si (100) substrate before (left) and after (right) O$_2$ plasma treatment. The sphere diameters reduced from 600 nm to 520 nm when exposed to an O$_2$ plasma for 25 seconds.

deposited close-packed PS sphere monolayer was then heated at 90 °C for 30 seconds to cause them to adhere better to the substrate surface without significantly deforming the spheres. The PS spheres were then O$_2$ plasma treated (Oxford Instruments Plasmalab 80Plus) at a power of 300 W, a pressure of 100 mbar, an oxygen flow rate of 50 sccm for 25 seconds to reduce the sphere diameter from 600 nm to ~520 nm allowing enough space between the spheres for a connected and mechanically stable ZnO nanoshell structure post-deposition. The nanostructured CeO$_2$ films are prepared on previously cleaned substrates by pulsed DC magnetron sputtering using the same deposition procedures to the ones described in refs 34 and 38. The process is repeated three times to yield a uniform CeO$_2$ thickness of 120 ± 10 nm.

For the CeO$_2$-coated ZnO films, the substrate is coated with approximately 40 layers of the 5 mM zinc acetate solution to yield a uniform ZnO film thickness of 80 ± 10 nm. The sample is then transferred to the sputtering chamber to deposit an approximately 50 ± 10 nm of nanostructured CeO$_2$ film on top of the ZnO. This resulted in a 120 ± 10 nm thick CeO$_2$-coated ZnO films to allow for a straight comparison study. The same process was repeated to fabricate the CeO$_2$-coated ZnO spherical nanoshells. A process flow chart is provided in Supplementary Figure II. Some CeO$_2$ films were also grown without ZnO, for the purposes of optical studies as mentioned below. These latter nanostructured CeO$_2$ films are prepared on previously cleaned substrates by pulsed DC magnetron sputtering using the same deposition procedures to the ones described in refs 34, 38. The process is repeated three times to yield a uniform CeO$_2$ thickness of 120 ± 10 nm. Table 1 summaries the sample structures used in this study and their associated labels.

Characterisation. The structural properties of the pure and CeO$_2$-coated ZnO samples were measured using a Bruker D8 Advance X-ray Diffractometer system with CuK$_\alpha$ radiation of wavelength $\lambda = 1.5418$ Å. The XRD measurements were carried out in locked coupled mode in a 2θ range from 20° to 60°. Sample morphology was studied using SEM (Karl-Zeiss EVO series and Hitachi S-5500 field emission (FE) SEM). The sample composition was studied using SIMS (Millbrook MiniSIMS Alpha). The optical absorption properties of the samples were studied at room temperature (RT) using a Perkin Elmer Lambda 40 UV-Vis spectrometer in the range from 200 to 800 nm with a resolution of 4 nm.

Results And Discussions

XRD Measurements. XRD patterns of the ZnO film (Z_F) and ZnO nanoshell (Z_NS); and, the CeO$_2$-coated ZnO film (C_Z_F) and CeO$_2$-coated ZnO nanoshell (C_Z_NS), as-deposited and annealed at 500 °C and 800 °C in air for 30 minutes are shown in Supplementary Figures III and IV, respectively. The XRD scans of all the Z_F, Z_NS, C_Z_F and C_Z_NS show that the crystalline quality of the samples is systematically improved as a result of annealing. The reflected x-ray intensity and reflection peak full width at half maximum (FWHM) of the CeO$_2$ (111) and ZnO (002) XRD peaks are used as an indicator of the crystallinity quality of the CeO$_2$ and ZnO deposits. The FWHM data is provided in Supplementary Table I and a detailed account of the XRD measurements is given in Supplementary section S1.
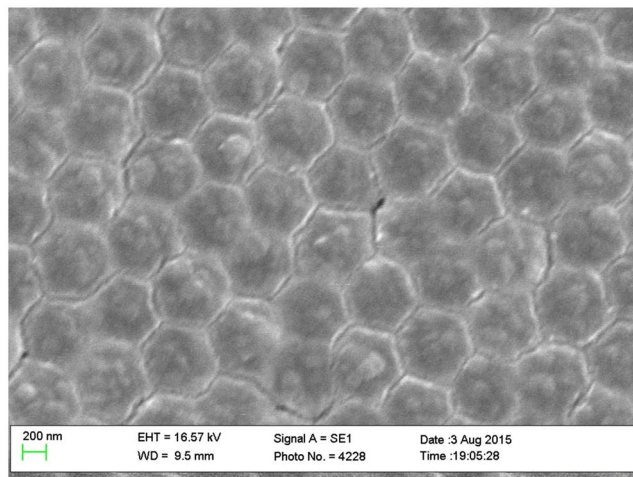
Figure 3. Plan view SEM image of the spherical Z_NS before complete removal of PS nanospheres i.e. samples were simply heated at 350 °C for 30 minutes to decompose the zinc acetate into zinc oxide.

SEM Measurements. Figure 2 shows SEM images of the PS sphere monolayer template, before and after the O_2 plasma treatment. As shown in Fig. 2(left), a PS sphere monolayer is observed on a Si (100) substrate without aggregation or multiple layer accumulation. Figure 2(right) clearly shows a reduction in the sphere diameters (from 600 nm to ~520 nm) after the O_2 plasma treatment, allowing enough space around the spheres for the Z_NS structures to fully interconnect during growth to ensure mechanical stability. There are some examples of slight movements of spheres, or of a sphere detaching, during the etch despite prior heating at 110 °C for 30 seconds to ensure good adherence, but these are very occasional and do not compromise the overall nanostructure integrity.

After the deposition of the zinc acetate films on the PS spheres, the structural morphology of the ZnO deposits depended on the post-deposition annealing temperature. Figure 3 shows a plan view of the zinc acetate decomposed into ZnO nanostructures by annealing the sample at 350 °C for 30 minutes. Spherical nano core-shell structures consisting of the PS sphere core and ZnO shells with a total diameter of ca.~60 nm are formed, as shown in Fig. 4. The thickness of the ZnO is estimated to be ~80 nm on the CeO_2-coated ZnO sample, as shown in the cross sectional view of the fractured nanostructures. Other views of the spherical nanostructures, after a complete removal of the PS spheres by carbonisation (i.e. by annealing at 500 °C for 30 minutes in air) and the addition of the thin CeO_2 film (~50 ± 10 nm thick), are also shown in Fig. 4.

Chemical composition measurements. Information on the chemical composition and impurity content in the samples were obtained by making SIMS measurements at different locations throughout the deposit. Supplementary Figure V shows the SIMS spectra of the C_Z_F in the mass region from 60 to 200 amu, at the boundary where the two materials meet. Sputtered CeO_2 SIMS spectra showed secondary ion peaks of Ce^+, CeO^+ and CeO_2^+[34]. As more scans are performed and the probing depth increased due to surface sputtering by the Ga ion beam, Zn^+ and ZnO^+ peaks start to appear and their intensity increased with the increase in the number of scans. Three different Zn isotopes are observed for the Zn ions, ^{64}Zn, ^{66}Zn and ^{68}Zn. These SIMS data clearly shows evidence of an abrupt interface between the ZnO and CeO_2 materials. Supplementary Figure VI presents the SIMS depth profiling data of the relative secondary ion emission yields ($^{64}Zn^+$, Ce^+, CeO^+ and CeO_2^+) as a function of depth at the boundary of the CeO_2-coated ZnO composite layers grown on Si(100) substrate. Further details on the SIMS measurements are provided in Supplementary section S2.

UV-Vis optical absorbance and directionality measurements. The optical properties of the as-deposited samples (CeO_2 film (C_F), Z_F, C_Z_F, Z_NS and C_Z_NS) were investigated by spectroscopic measurements. As mentioned above, the optical absorbance spectra of the films deposited on quartz substrates are recorded in the wavelength range from 200 to 800 nm. Typical absorbance curves for the films grown on quartz are shown in Fig. 5. The influence of adding a CeO_2 film on top of the ZnO film is clearly observed in these absorbance spectra. The C_Z_F have high absorption in the UV and visible regions followed by a fall-off in the absorption at wavelengths greater than approximately 380 nm. Both pure C_F and Z_F (with approximately the same film thickness of 120 ± 10 nm) have lower absorbance in the visible region and the absorbance spectra of the composite C_Z_F seems to be due to the joint effects of the two constituent oxides. Adding CeO_2 to the ZnO films clearly increases the absorption in the UV spectral region.

Figure 6 shows the UV-Vis absorption spectra of the pure Z_F, C_Z_F, Z_NS and C_Z_NS samples, with the same physical thicknesses of the two materials in both the film and nanoshell morphologies. All samples are annealed at 500 °C in air for 30 minutes in order to completely eliminate the PS spheres from the nanoshell samples and to enable a direct comparison between the nanoshells and the films. Other Z_F, C_Z_F, Z_NS and C_Z_NS samples were also annealed at 800 °C to crystallise the materials; however no significant differences in absorption, compared to samples annealed at 500 °C, are seen in these samples. It can be clearly seen in Fig. 6 that pure Z_NS and C_Z_NS samples exhibit a much higher UV light absorption level of ~3 times and 1½ times
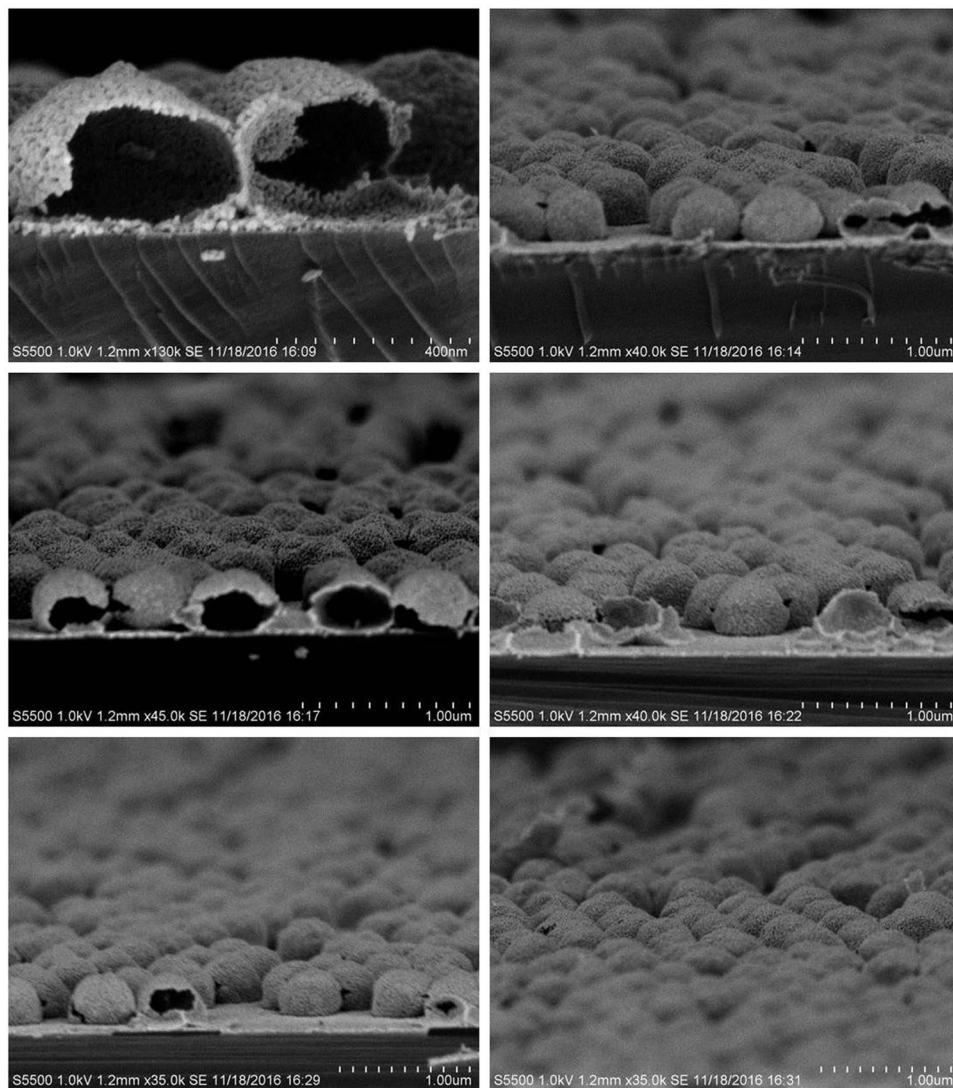
Figure 4. FE-SEM images of the spherical nanoshell structures after the removal of the PS spheres (i.e. annealed at 500 °C for 30 minutes in air). The samples are deposited on both Si (100) and quartz substrates. The SEM images show 90° view of the Z_NS structures at different positions, with clear evidence of internal voids following PS sphere removal.
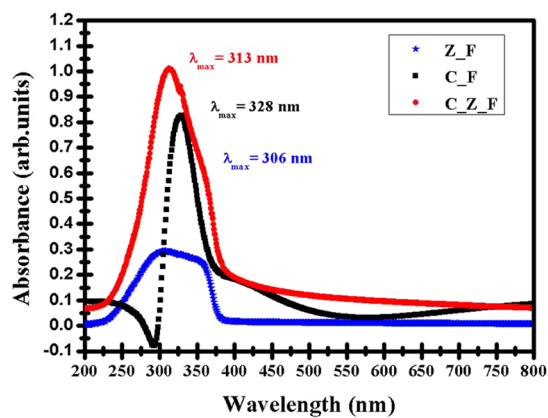

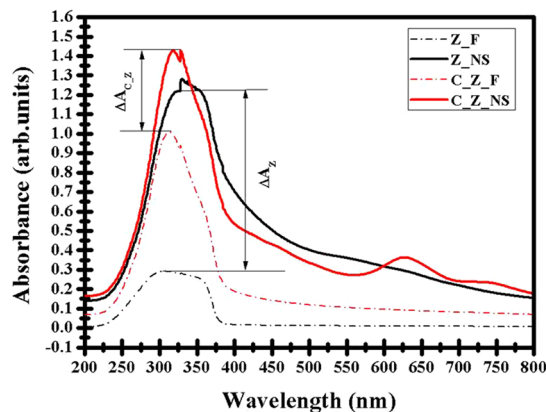**Figure 5.** Room temperature UV-Vis absorption spectra of Z_F, C_F and C_Z_F (thickness ~120 ± 10 nm) on quartz substrates.

Figure 6. Room temperature UV-Vis absorption spectra of Z_F, Z_NS C_Z_F and C_Z_NS samples, under normal incidence, with a clear indication of an increase in the absorption (ΔA) as a result of the nanoshell structure.
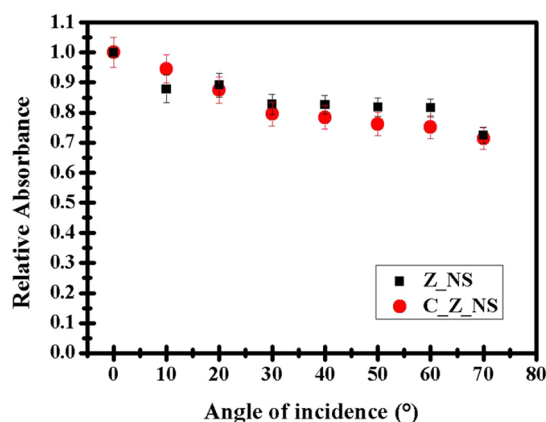

Figure 7. Integrated relative absorbance for different incidence angles relative to normal incidence.

the comparable thin film absorption, respectively. This confirms that a significant enhancement in the UV light absorption is achieved by the engineered spherical nanoshells, for identical sample material thicknesses; hence the geometry of the structure dramatically improves the absorption. It is important to note that the discontinuity at ~330 nm is due to an instrumental artefact (change in grating response) and it is detected in most of our UV-Vis absorption spectra. The samples with the nanoshell morphologies also show distinctly higher apparent absorption in the visible region, compared to equivalent thickness samples with thin film morphologies. We believe that this is due to the effects of increased light scattering and diffraction of energy out of the incident beam, due to the ordered spherical nanoshells structure, which has a periodicity of similar order (600 nm) to visible light wavelengths.

The absorbance enhancement is also relatively insensitive to the angle of incidence, as shown in Fig. 7. Spectrally integrated over the wavelength range of 200–800 nm, the relative absorbance enhancement shows a maximum variation of less than 30% between values measured at normal incidence and at an incidence angle of 70° from the normal for both the C_Z_NS and Z_NS samples, compared to the relevant thin film samples. The relative absorbance enhancement at an angle i is calculated using the following formula:

$$\text{Relative Absorbance Enhancement }(i) = \frac{I_{A\_i}}{I_{A\_0°}} \tag{1}$$

$I_{A\_0°}$ and I_{A_i} are the spectrally integrated absorbance enhancements at normal incidence and an incidence angle of i from the normal, respectively. The spectrally integrated absorbance enhancement at all incident angles was determined using:

$$I_{A\_i} = I_{A_i}(NS) - I_{A_i}(F) \tag{2}$$

where $I_{A_i}(NS)$ and $I_{A_i}(F)$ are the spectrally integrated absorbances for the nanoshell and thin film samples (at an incidence angle of i) with the same physical thicknesses of the materials in both the film and nanoshell morphologies.

Conclusions

In this paper, we have demonstrated a simple and reproducible method to fabricate ZnO and CeO_2-coated ZnO thin films and functional nanoshell nanostructures on Si (100) and quartz substrates. The ZnO films and nanostructures were grown by a facile drop coating method using zinc acetate in anhydrous ethanol solution as a starting material while the CeO_2 deposits were produced by a pulsed DC magnetron sputtering method. XRD, SEM and SIMS measurements were used to confirm the structural, morphological and compositional properties of the deposited materials. In particular XRD data indicated the poorly crystalline nature of the as-deposited ZnO and CeO_2 nanostructures and showed that the crystalline quality improved after post-deposition annealing at higher temperatures. SEM images showed the successful engineering of the spherical nanoshell structures with a clear indication of the central voids. SIMS analysis of the chemical composition showed the presence of the Ce^+, CeO^+, CeO_2^+, Zn^+ and ZnO^+ ionic species in the various relevant samples as well as the three different Zn isotopes (^{64}Zn, ^{66}Zn and ^{68}Zn), and depth profiling showed the location of the ZnO/CeO_2 interface in relevant samples. UV and visible light absorption was very significantly enhanced through the engineering of spherical nanoshells on a PS monolayer template, most likely due to the whispering gallery modes in such nanoshell cavities, as well as the addition of the CeO_2 layer. Our results and analysis clearly show that key materials properties such as the UV and visible light absorption can be significantly enhanced by nanostructure engineering of the deposits to create spherical nanoshell cavities. These results may prove very useful in terms of enabling future materials and device developments, with the aim of controlling key deposit parameters for technologically important applications, in particular in the areas of solar-thermal fuel generation and catalysis, where the combination of the nanostructure engineering possible with ZnO and the oxygen storage and variable stoichiometry properties of CeO_2 provides a unique set of advantageous deposit properties.

References

1. Yao, Y. *et al.* Broadband light management using low-Q whispering gallery modes in spherical nanoshells. *Nature communications* **3**, 664 (2012).
2. Brongersma, M. L., Cui, Y. & Fan, S. Light management for photovoltaics using high-index nanostructures. *Nature materials* **13**, 451–460 (2014).
3. Leung, S.-F. *et al.* Light management with nanostructures for optoelectronic devices. *The Journal of Physical Chemistry Letters* **5**, 1479–1495 (2014).
4. Faisal, M. *et al.* Role of ZnO-CeO$_2$ nanostructures as a photo-catalyst and chemi-sensor. *Journal of Materials Science & Technology* **27**, 594–600 (2011).
5. de Lima, J. F., Martins, R. F., Neri, C. R. & Serra, O. A. ZnO: CeO$_2$-based nanopowders with low catalytic activity as UV absorbers. *Applied Surface Science* **255**, 9006–9009 (2009).
6. Chockalingam, R., Amarakoon, V. R. & Giesche, H. Alumina/cerium oxide nano-composite electrolyte for solid oxide fuel cell applications. *Journal of the European Ceramic Society* **28**, 959–963 (2008).
7. Li, R. *et al.* UV-shielding properties of zinc oxide-doped ceria fine powders derived via soft solution chemical routes. *Materials Chemistry and Physics* **75**, 39–44 (2002).
8. Chueh, W. C. *et al.* High-flux solar-driven thermochemical dissociation of CO$_2$ and H$_2$O using nonstoichiometric ceria. *Science* **330**, 1797–1801 (2010).
9. Ge, C., Xie, C. & Cai, S. Preparation and gas-sensing properties of Ce-doped ZnO thin-film sensors by dip-coating. *Materials Science and Engineering: B* **137**, 53–58 (2007).
10. Yabe, S. & Sato, T. Cerium oxide for sunscreen cosmetics. *Journal of Solid State Chemistry* **171**, 7–11 (2003).
11. Tsunekawa, S., Wang, J.-T., Kawazoe, Y. & Kasuya, A. Blueshifts in the ultraviolet absorption spectra of cerium oxide nanocrystallites. *Journal of applied physics* **94**, 3654–3656 (2003).
12. Montemor, M., Pinto, R. & Ferreira, M. Chemical composition and corrosion protection of silane films modified with CeO$_2$ nanoparticles. *Electrochimica Acta* **54**, 5179–5189 (2009).
13. Jagadish, C. & Pearton, S. J. Zinc oxide bulk, thin films and nanostructures: processing, properties, and applications. (Elsevier, 2011).
14. Torres-Huerta, A. *et al.* Preparation of ZnO: CeO$_2$−x thin films by AP-MOCVD: Structural and optical properties. *Journal of Solid State Chemistry* **183**, 2205–2217 (2010).
15. Nair, S. *et al.* Role of size scale of ZnO nanoparticles and microparticles on toxicity toward bacteria and osteoblast cancer cells. *Journal of Materials Science: Materials in Medicine* **20**, 235–241 (2009).
16. Kalpana, D., Omkumar, K., Kumar, S. S. & Renganathan, N. A novel high power symmetric ZnO/carbon aerogel composite electrode for electrochemical supercapacitor. *Electrochimica Acta* **52**, 1309–1315 (2006).
17. Byrne, D. *et al.* Study of morphological and related properties of aligned zinc oxide nanorods grown by vapor phase transport on chemical bath deposited buffer layers. *Crystal Growth & Design* **11**, 5378–5386 (2011).
18. Hughes, W. L. & Wang, Z. L. Controlled synthesis and manipulation of ZnO nanorings and nanobows. *Applied Physics Letters* **86**, 043106 (2005).
19. Wan, Q. *et al.* Fabrication and ethanol sensing characteristics of ZnO nanowire gas sensors. *Applied Physics Letters* **84**, 3654–3656 (2004).
20. Kong, X. Y. & Wang, Z. L. Polar-surface dominated ZnO nanobelts and the electrostatic energy induced nanohelixes, nanosprings, and nanospirals. *Applied physics letters* **84**, 975–977 (2004).
21. Wang, X. *et al.* ZnO Hollow Spheres with Double-Yolk Egg Structure for High-Performance Photocatalysts and Photodetectors. *Advanced Materials* **24**, 3421–3425 (2012).
22. He, C. X. *et al.* Sonochemical Preparation of Hierarchical ZnO Hollow Spheres for Efficient Dye-Sensitized Solar Cells. *Chemistry-A European Journal* **16**, 8757–8761 (2010).
23. Rasmussen, J. W., Martinez, E., Louka, P. & Wingett, D. G. Zinc oxide nanoparticles for selective destruction of tumor cells and potential for drug delivery applications. *Expert opinion on drug delivery* **7**, 1063–1077 (2010).
24. Zhang, Z. *et al.* ZnO hollow nanofibers: fabrication from facile single capillary electrospinning and applications in gas sensors. *The Journal of Physical Chemistry C* **113**, 19397–19403 (2009).
25. Liu, J. *et al.* Yolk/shell nanoparticles: new platforms for nanoreactors, drug delivery and lithium-ion batteries. *Chemical Communications* **47**, 12578–12591 (2011).
26. Dong, Z. *et al.* Accurate Control of Multishelled ZnO Hollow Microspheres for Dye-Sensitized Solar Cells with High Efficiency. *Advanced materials* **24**, 1046–1049 (2012).
27. Sun, Z. *et al.* Fish-scale bio-inspired multifunctional ZnO nanostructures. *NPG Asia Materials* **7**, e232 (2015).
28. Sun, Z. *et al.* Fly compound-eye inspired inorganic nanostructures with extraordinary visible-light responses. *Materials Today Chemistry* **1–2**, 84–89 (2016).

29. Sun, Z. *et al.* Architecture designed ZnO hollow microspheres with wide-range visible-light photoresponses. *Journal of Materials Chemistry C* **1**, 6924–6929 (2013).
30. Li, Q. *et al.* Template-free polyoxometalate-assisted synthesis for ZnO hollow spheres. *Journal of Solid State Chemistry* **182**, 1149–1155 (2009).
31. Shen, G., Bando, Y. & Lee, C.-J. Synthesis and evolution of novel hollow ZnO urchins by a simple thermal evaporation process. *The Journal of Physical Chemistry B* **109**, 10578–10583 (2005).
32. Deng, C., Hu, H., Shao, G. & Han, C. Facile template-free sonochemical fabrication of hollow ZnO spherical structures. *Materials Letters* **64**, 852–855 (2010).
33. Byrne, D., McGlynn, E., Cullen, J. & Henry, M. O. A catalyst-free and facile route to periodically ordered and c-axis aligned ZnO nanorod arrays on diverse substrates. *Nanoscale* **3**, 1675–1682 (2011).
34. Eltayeb, A. *et al.* Control and enhancement of the oxygen storage capacity of ceria films by variation of the deposition gas atmosphere during pulsed DC magnetron sputtering. *Journal of Power Sources* **279**, 94–99 (2015).
35. Greene, L. E. *et al.* Low-temperature wafer-scale production of ZnO nanowire arrays. *Angewandte Chemie International Edition* **42**, 3031–3034 (2003).
36. Greene, L. E. *et al.* General route to vertical ZnO nanowire arrays using textured ZnO seeds. *Nano Letters* **5**, 1231–1236 (2005).
37. Byrne, D. The growth and characterisation of ordered arrays of zinc oxide nanostructures and optical studies of defects in zinc oxide PhD thesis, Dublin City University (2012).
38. Eltayeb, A. *et al.* Control of crystal structure, morphology and optical properties of ceria films by post deposition annealing treatments. *Thin Solid Films* **603**, 363–370 (2016).

Acknowledgements

Author Contributions

A.E. prepared the samples, conducted the experiments, analysed the data and helped to write the paper, including taking main responsibility for the preparation of the first draft. E.McG. helped to write the paper, particularly later drafts. E. McG. and S.D. designed the research and supervised the experiments. All authors revised the manuscript.

Additional Information

Supplementary information accompanies this paper at doi:10.1038/s41598-017-03905-4

Competing Interests: The authors declare that they have no competing interests.

Publisher's note: Springer Nature remains neutral with regard to jurisdictional claims in published maps and institutional affiliations.